



High responsivity, self-powered carbon–zinc oxide hybrid thin film based photodetector

H. Ahmad^{1,2} · T. Tamil¹

Received: 22 May 2018 / Accepted: 5 July 2018 / Published online: 13 July 2018
© Springer-Verlag GmbH Germany, part of Springer Nature 2018

Abstract

A self-powered n-Si/C–ZnO/SiO₂/p-Si heterojunction photodetector (PD) which comprises of carbon (C) and zinc oxide (ZnO) nanostructures on a n-type silicon (n-Si) substrate was prepared via vapor phase transport method. Excellent photodetection under 468 nm light illumination for powers ranging from 2.78 to 2910 μW delivered a quick response of about 9.5 μs. A high photoresponsivity of 2.082/AW and external quantum efficiency about 551% were obtained. The mechanism involved for the generation of a photocurrent at a zero bias voltage was discussed for future energy efficient optoelectronics devices. The morphology and composition of C, Zn and O were confirmed by field emission scanning electron microscope, energy dispersive X-ray and Raman scattering analysis. The formation of ZnO nanowires range from 10 to 100 nm, aided by the photoconduction mechanism. The Raman E_2^{high} mode of 437/cm of ZnO and the presence of D and G bands show the formation of a hybrid C–ZnO thin film. The calculated rectifying ratio is found to shift as the direct current bias voltage and light power increased. The deposition of C particles on the ZnO surface creates point defects and sub-energy levels in the ZnO bandgap which favour fast responsivity in the PD.

Keywords Self-powered · Photodetector · Carbon · Zinc oxide · Responsivity

Introduction

Recent advances in the field of one-dimensional (1D) and two-dimensional (2D) nanostructures have seen the development and enhancement of many opto-electronic devices for various applications. In particular, the enhancement of 1D and 2D nanostructures onto signal processing devices, especially self-powered PDs have been the focus of intense research efforts. These devices, which can convert incident photons into an electrical signal can be integrated with other devices to enhance functionality due to their ability to operate without a power source. This is due to the built-in potential difference that permits the self-powered PDs to be integrated with external units to enhance the functionality. Furthermore, these 1D and 2D materials allow for the strong interaction of photons through polaritons (Liu et al.

2014), giving these devices significant advantages including small device size, energy saving and the ability to operate in extreme conditions (Garnier et al. 2015). However, 1D ZnO nanostructures such as nanotubes (NTs), nanowires (NWs) and nanoribbons (NRs), which exhibits length to width aspect ratios more than 1000 are promising candidates for highly sensitive PDs (Zhai et al. 2010b). This is due to the inherent properties of ZnO such as chemical stability (Radisavljevic et al. 2011), direct wide bandgap of 3.37 eV (Wang 2004), high electron mobility of 2000 cm²/(Vs) at 80 K (Wagner and Helbig 1974), large exciton binding energy of 60 meV, strong room temperature luminescence (Jagadish and Pearton 2011) and highly efficient light absorption and piezoelectricity that are important factors in developing next generation transparent and wearable ZnO PDs (Koppens et al. 2014; Lopez-Sanchez et al. 2013). Furthermore, hybrid ZnO materials have made self-powered photodetection a significant possibility. The incorporation of ZnO with graphene layers a few atoms thick would allow electrons free movement in the 2D plane but restricted in moving a third direction, as governed by quantum mechanics (Low et al. 2014; Teng et al. 2017).

✉ H. Ahmad
harith@um.edu.my

¹ Photonics Research Centre, Faculty of Science, University of Malaya, 50603 Kuala Lumpur, Malaysia

² Department of Physics, Faculty of Science and Technology, Airlangga University, Surabaya 60115, Indonesia

Various methods and techniques such as physical and chemical vapor deposition (Zhao et al. 2017), thermal evaporation (Chrissanthopoulos et al. 2011), vapour phase transport (VPT) (Thandavan et al. 2014b), facile co-precipitation (Kumar and Sharma 2017) and sol-gel (Mridha and Basak 2007) have been utilized to fabricate hybrid ZnO nanoparticles (NPs). Nusir and Manasreh (2015) demonstrated good photoconduction from fabricated metal-semiconductor, near infrared (NIR) self-powered PDs which consisted of gold (Au) and titanium (Ti) electrodes with spacings of 5, 10 and 50 μm on a semi-insulating layer of gallium arsenide (GaAs). However, the reported recovery time is approximately 0.19 s, a somewhat high value even though the proposed PD shows a significant increase in its external quantum efficiency (EQE) and photoresponsivity to infrared (IR) light at 800 nm with a zero bias voltage. A better response time and photoresponsivity of 2 ms and 1.52/AW were obtained by Li et al. (2016) under the 600 nm illumination on a self-powered PD using a p-n vertical heterojunction formed from reduced graphene oxide/n-Si. A self-powered nano-heterojunction PD consisting of a $\text{Ag}_2\text{S}/\text{ZnO}$ core-shell prepared by a wet chemical method was shown to deliver a slightly slower response time of 5 ms but with a wider spectral response ranging from 400 to 1100 nm due to its energetically favourable fermi level alignment and efficient hole transporting property (Chen et al. 2018). Ouyang et al. (2018) showed that the enhancement of the photocurrent at a zero bias voltage was due to pyroelectric-polarization and a thermos-potential that alternatively acts as heterojunctions in the PD, leading to a wide photoresponse range and tunable spectral selectivity. Ning et al. (2018) reported a higher ON-OFF ratios of up to 2.5×10^4 are achieved in a self-powered Ag doped ZnO nanofiber PD at UV illumination of 360 nm, attributed to the presence of Ag NPs that improves the response time as well. In this regard, oxygen (O) independency, high sensitivity and fast response times are anticipated in these ZnO based self-powered PDs. The presence of ZnO NWs improves the photoresponsivity effects by increasing the active surface area. Chen et al. (2014) demonstrated enhanced photoresponsivity of about 20/mAW in a ZnO film self-powered PD based on an asymmetric pair of Au electrodes using UV illumination of 365 nm, which is achieved by decreasing the finger width of the Au electrodes. The PD also exhibits a very profound short response and decay time about 0.71 and 4 μs . Yu et al. (2017) established a promising way to fabricate inorganic/organic self-powered PD that exhibited a responsivity of 120/mAW with a rise and fall time, respectively, at 4.5 μs and 2.84 ms. Self-powered, solar-blind PDs based on ZnO heterostructures with gallium oxide show an ultrahigh responsivity of about 9.7/mAW under illumination at 251 nm which has a high UV/visible rejection ratio and cut off wavelength of 266 nm (Zhao et al. 2017). The importance of Schottky contacts in the PD was discussed

by Van Schalkwyk et al. (2012) in which increased photoresponsivity from 40 to 52/mAW was attained after a gold (Au) probe was placed in contact with Iridium oxide (IrO_2) on a solar-blind UV aluminium gallium nitride (AlGaN) PD.

This article accounts for a self-powered carbon-ZnO (C-ZnO) hybrid heterojunction PD. The proposed PD is fabricated by a n-Si/C-ZnO hybrid thin layer with a $\text{SiO}_2/\text{p-Si}$ substrate. As expected, the VPT method allows for the incorporation of C particles on the surface of the ZnO NWs using a built-in electric field (Zhang et al. 2018). Photodetection of light at 468 nm and 2910 μW at a zero bias voltage, gives a quick response of about 9.5 μs , high responsivity of 2.082/AW and EQE of about 551% are obtained. This performance is comparable to that of reported ZnO hybrid PDs, giving promise for the development of optoelectronic devices.

Experimental setup

The fabrication of the self-powered PDs uses the VPT technique to enable the growth of C-ZnO hybrid nanostructures on an n-Si wafer. The n-Si wafer was cut into a chip 1 cm \times 1 cm and ultrasonically cleaned in a 10% hydrofluoric (HF) acid bath solution for 30 min to remove the oxide layer from the substrate. The substrate is then rinsed thoroughly in deionised (DI) water to remove any HF stains and cleaned again ultrasonically in an acetone bath solution for 1 h. After an hour, the substrate is rinsed in DI water to remove any acetone stains on the n-Si substrate before being blown immediately with nitrogen (N_2) gas for a fast drying. The pre-treated, bare n-Si substrate was placed in the vacuum chamber as shown in Fig. 1a for the deposition of the C-ZnO hybrid thin film (Thandavan et al. 2014a) for 25 min, with brass used as a Zn source. The brass was heated by a hot filament between 500 and 600 $^\circ\text{C}$ over a deposition period of 25 min. Simultaneously, argon (Ar) gas, allowed to flow at 50 sccm through a methanol solution was used as a source of C and O to form the C-ZnO hybrid thin film. Immediately after the deposition period, the hot filament is switched off although the Ar gas still injected into the system, only this time without being channelled through the methanol solution first. At the same time, the temperature of the sample is slowly reduced until it reaches room temperature. Once this happens, the Ar gas is removed, and the sample heated again on a hotplate to a temperature of 400 $^\circ\text{C}$ to oxidize any excess C layers on the C-ZnO hybrid thin film. The prepared C-ZnO thin film is then held against an $\text{SiO}_2/\text{p-Si}$ substrate using a paper clip, while silver (Ag) conducting paste was applied at the n-Si and p-Si junctions to form the source and drain electrodes, respectively, as shown in Fig. 1b.

A light source with a luminescence spectrum as shown in Fig. 1c was used to illuminate onto the fabricated PD. The spectrum revealed a dominant sharp peak at 468 nm

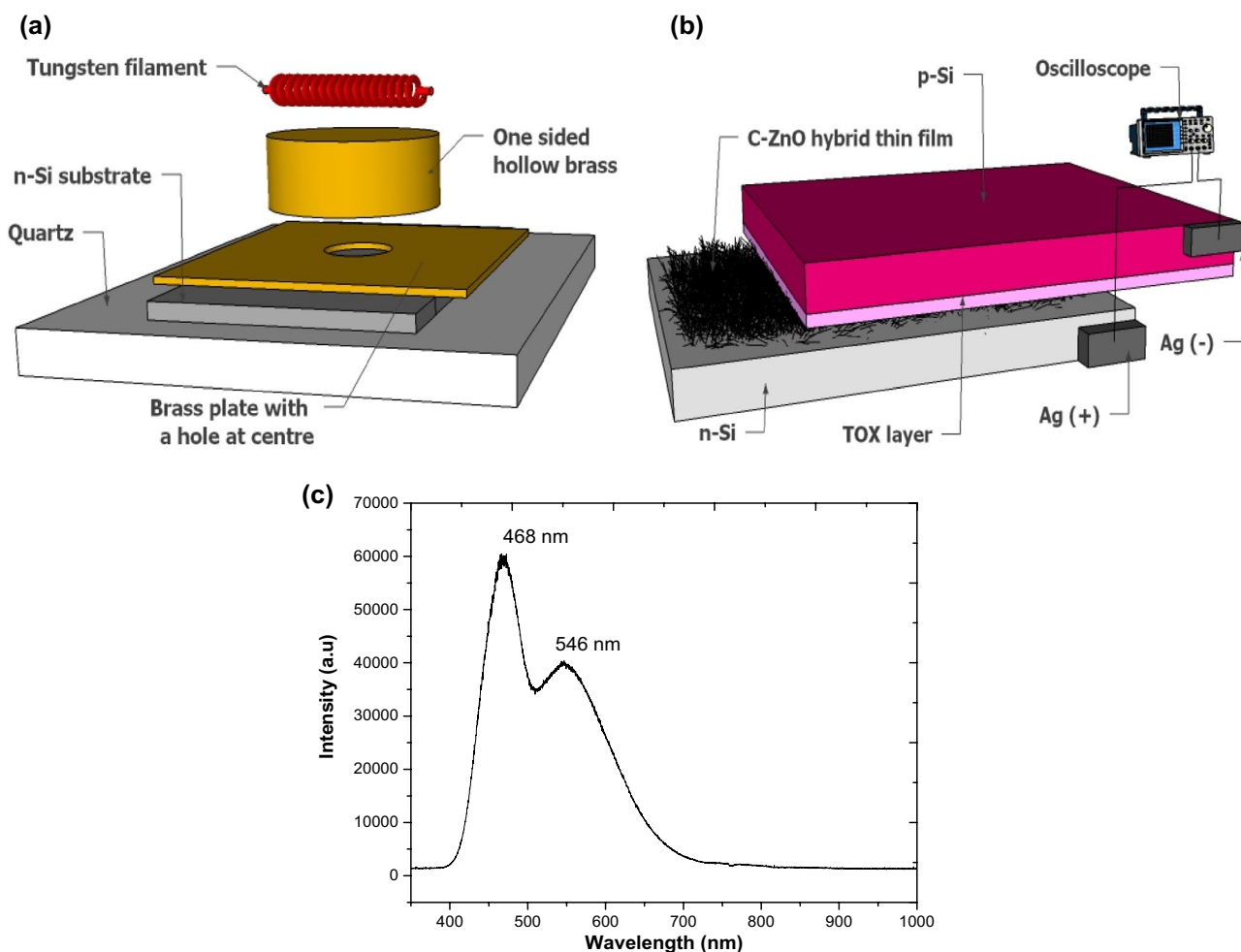


Fig. 1 **a** Schematic diagram of experimental setup, showing from the bottom the Quartz plate, n-Si layer, brass plate with a hole, one sided hollow brass plate and tungsten filament, **b** C–ZnO hybrid thin

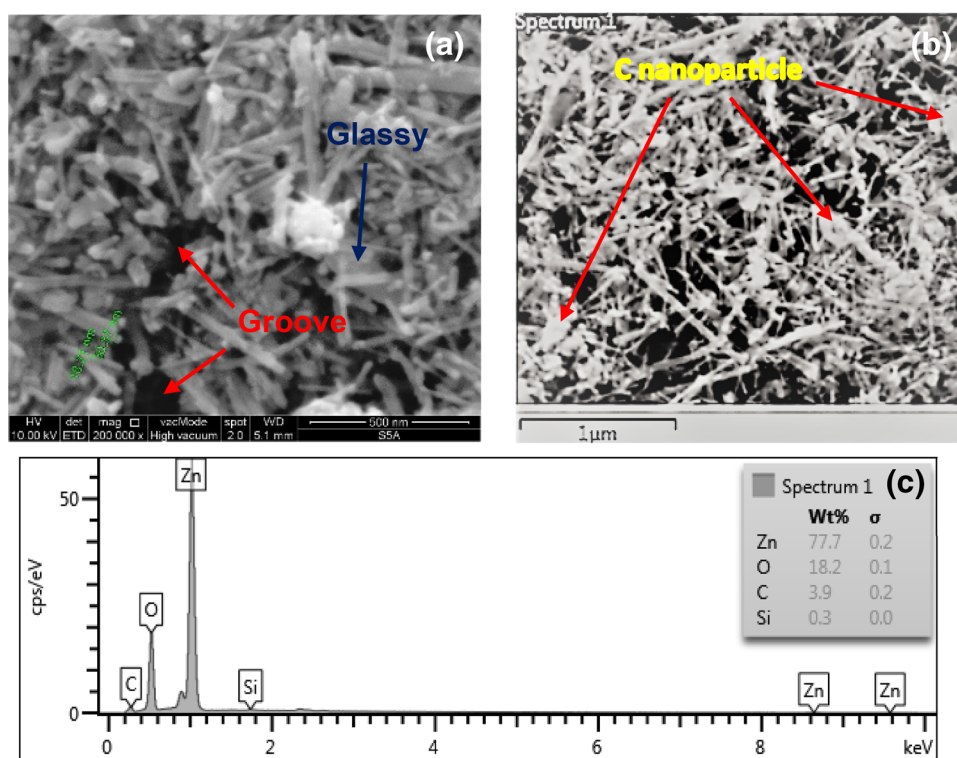
film clamped onto the SiO₂/p-Si layer and **c** luminescence spectrum obtained from the illuminated C–ZnO surface area

and small broad shoulder at around 546 nm for the light. The photoconduction characteristic of the C–ZnO hybrid thin film was determined with the illumination source at fixed distance of 1 cm from the surface of the PD. The current–voltage (*I–V*) characteristics were collected for a DC bias voltage range of – 4 to +4 V using a Keithley 2410 Source Meter unit, while the power of the light beam reaching the PD perpendicular to the active area is measured using a S130VC slim photodiode power sensor. The power of the illumination source is controlled by varying its input voltage supply, and frequency modulation is obtained through the use of a DS34530 MHz Synthesized Function Generator. Measurement of the PD’s response to the modulated signal, in particular its temporal response and photoresponsivity rise (τ_r) and fall (τ_f) time was done using a Yokogawa DLM2054 mixed signal oscilloscope for. All measurements were performed at room temperature under ambient conditions.

FESEM and EDX analysis

A Quanta 450 FEG scanning electron microscope (SEM) was utilized to obtain the morphology and composition of the hybrid C–ZnO coated n-Si thin film. From Fig. 2a it can be seen that the fabricated NWs are between 18 and 32 nm in diameter, with an average length to diameter ratio of 10. The NWs were observed to be dense and unevenly distributed on the substrate, resulting in ‘grooves’ on the substrate layer. The surface structure of the ZnO NWs have a long cylindrical shape, with the formation of C particles not clearly observable as their bonding to the surface of the NWs results in a non-hexagonal ZnO structure. The formation of a thin glassy layer, believed to be C particles is also observed in Fig. 2a. ZnO NWs smaller than 18 nm in diameter and approximately 200 nm long are seen in the scans shown in Fig. 2a. The EDX results in Fig. 2c, with the relevant (SEM) scanned area shown in Fig. 2b shows a larger

Fig. 2 **a** FESEM image of C–ZnO hybrid thin film, **b** FESEM image of larger scanned area showing distribution of C NPs and ZnO NWs, and **c** EDX scan results



of C–ZnO hybrid thin film area in which the distribution of C NPs on the surface of the ZnO NWs can be better seen. The EDX result gives the C, Zn and O elemental composition at respective weight percentages of 3.9, 18.2 and 77.7 on the n-Si substrate. Spots in the image are attributed to C particles that form on the surface of ZnO NWs, with the C–ZnO hybrid film that was formed on the n-Si substrate being thin enough to allow for the detection of Si as well, at a weight 0.3%. The presence of C NPs on the ZnO NWs thin film was due to the evaporation of the methanol solution which is subsequently transported and diffused on the n-Si substrate (Thandavan et al. 2014a).

Raman scattering spectrum and XRD analysis

Figure 3a shows the Raman scattering spectrum of the C–ZnO hybrid thin film as obtained from Renishaw in-via Raman microscope. Both the non-resonant and resonant Raman scattering measurements are obtained in a back-scattering geometry with an unpolarized light source. Peaks are observed at 332, 437, 576, 976 and 1155/cm and can be related to the Raman vibrational modes of ZnO. A prominent sharp peak in the expected low frequency region of the Si peak at 437/cm is assigned to the E_2^{high} mode of hexagonal ZnO due to its heavy Zn sublattice (Kumar et al. 2006). Another small peak at 332/cm is attributed to the

$E_2^{\text{high}}-E_2^{\text{low}}$ vibrational mode of O atoms in ZnO (Rajalakshmi et al. 2000) while a small perturbation at is observed at 576/cm, which is close to $A_1(\text{LO})$ mode in the resonance Raman spectra of ZnO quantum dots (Ye et al. 2009). In the higher frequency region, a sharp peak at 976/cm can be associated to the A_1 symmetry of the 2TO modes which corresponds to the $L-M-K-H$ Brillouin zone lines. The noticeable peak at 1155/cm can also be related to ZnO as shown in Fig. 3. This is due to $2A_1(\text{LO})$, $2E_1(\text{LO})$ and 2LO vibrational modes at Brillouin zone point Γ and $A-L-M$ lines. Dominant and sharp peaks at 521/cm are attributed to the first order of the Si peak which further confirms that the C–ZnO hybrid film is thin enough to allow the penetration of green laser 532 nm to the substrate layer (Khorasaninejad et al. 2012; Scott 1970). The first order Raman absorption of the disordered D and G band are obtained at 1364 and 1578/cm, respectively (Sahatiya and Badhulika 2015). The fabricated C–ZnO film is dominated by the sp^2 orbital due to the resonance of visible excitation with the π sites. Therefore, even for carbon atoms with highly bonded sp^3 orbital, the Raman spectra are still visible due to sp^2 vibrations (Ferrari 2007). The G peak arises is due to the stretching of all of sp^2 atoms pairs, while the D peak is due to breathing modes of the sp^2 orbitals (Castiglioni et al. 2001; Ferrari et al. 2006).

The XRD profile of C–ZnO as shown in Fig. 3b is compared and indexed with the standard peaks of hexagonal wurtzite ZnO as given in JCP2.2CA: 00-036-1451 card. Three dominant high intensity peaks that are related to plane indices of

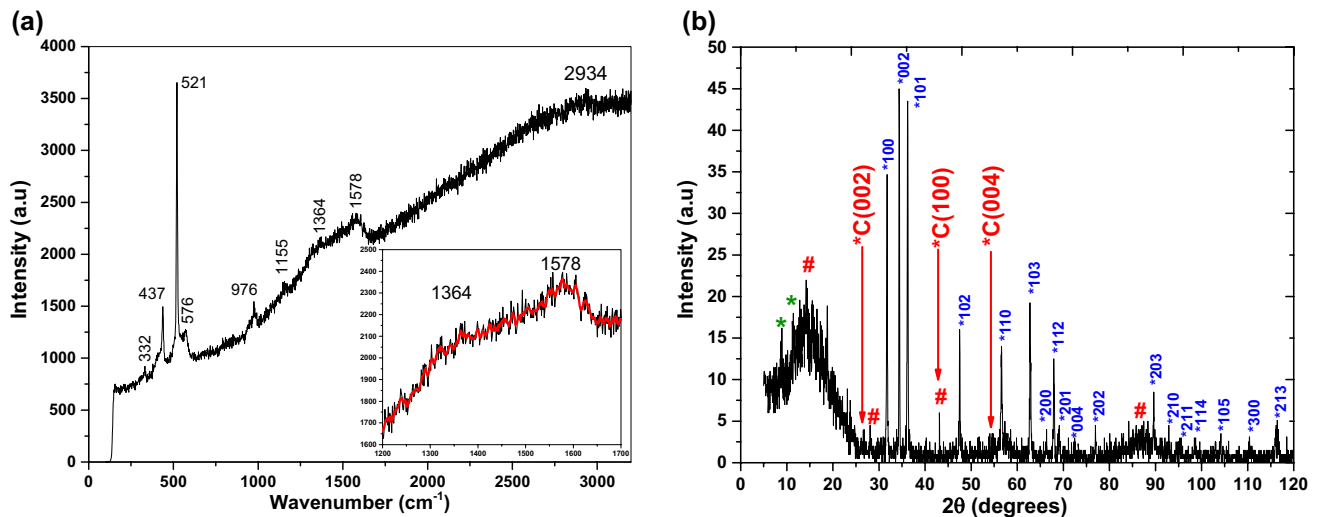


Fig. 3 **a** Raman scattering spectrum and **b** XRD spectrum of the fabricated C–ZnO hybrid thin film. The XRD measurements were taken three times for repeatability, with each reading giving the same peak values

d100, d002 and d101 are noticeable at 31.7° , 34.4° and 36.2° , respectively. The strong peak at $\langle 002 \rangle$ preferred orientation in *c*-axis is predictable. Other than that, low intensity peaks at 47.3° (d102), 56.5° (d110), 62.9° (d103), 66.5° (d200), 67.9° (d112), 69.4° (d201), 76.4° (d202), 88.3° (d203), 98.6° (d114), 104.1° (d105) and 116.4° (d213) also noticeable in Fig. 3b. However, compared to the previous studies by Ahmad et al. (2017), this XRD spectrum found is be more intense due to the prolonged deposition period of up to 25 min and further heating on the hotplate at 400°C , allowing for the oxidation of excess C layers on the fabricated C–ZnO hybrid thin film, and thus the detection of weak peaks. Furthermore, the profound broad peak at 14.4° can be related to shifted graphitic oxide (Brownson and Banks 2010) which is possibly due to the strain distribution in the sample during the heating process and during the deposition of C–ZnO hybrid layer in the vacuum chamber. The broad range of the peak can be related to an appearance of other C related peaks preferably graphene oxide at 8.76° and 11.4° . C peaks of C_{002} , C_{100} and C_{004} are also clearly identified at 26.7° , 43.1° and 54.5° (Huang et al. 2017), while an additional peaks at 28.1° and 43.1° indicating the presence of crystalline graphene oxide in the sample (Liou and Huang 2014; Niu et al. 2016). The presence of C related peaks and the broad shoulder indicates that the proposed fabrication technique allows for the deposition of C particles on the walls of ZnO NPs, even though the presence of C is not clearly noticeable from the FESEM images.

I–V characterization

The effect of illumination on the electrical transport of the PD is investigated by measuring the *I–V* characteristics of the PD under dark and illuminated conditions at powers of 2.01, 2.78, 12.5, 973, 2042 and 2910 μW as shown in Fig. 4a. A 468 nm light source was used to illuminate the whole C–ZnO hybrid thin film exposed area. Under dark and illuminated conditions, the *I–V* curves clearly indicate nonrectifying behavior which is consistent with the Schottky contact between the Ag electrodes, C–ZnO hybrid thin film and $\text{SiO}_2/\text{p-Si}$ substrate. Good Schottky junction behaviour and the stability of the induced photocurrent at zero bias voltage is analysed as in Fig. 4c. The analysis reveals the distribution of a photocurrent from a self-powered C–ZnO hybrid PD without any external electric field across the Ag source and drain electrodes. The increase in the photocurrent corresponds well to the rising illumination powers ranging from 2.01 to 2910 μW , and is believed to be a result of the attraction of positive charge carriers in the opposite Schottky junction to the photogenerated electrons. Due to the light illumination at the C–ZnO and n-Si Schottky junction, electron and hole (*e–h*) pairs were generated and driven by the inner electric field. This enables the movement of photoelectrons from the n-Si region through an external circuit to

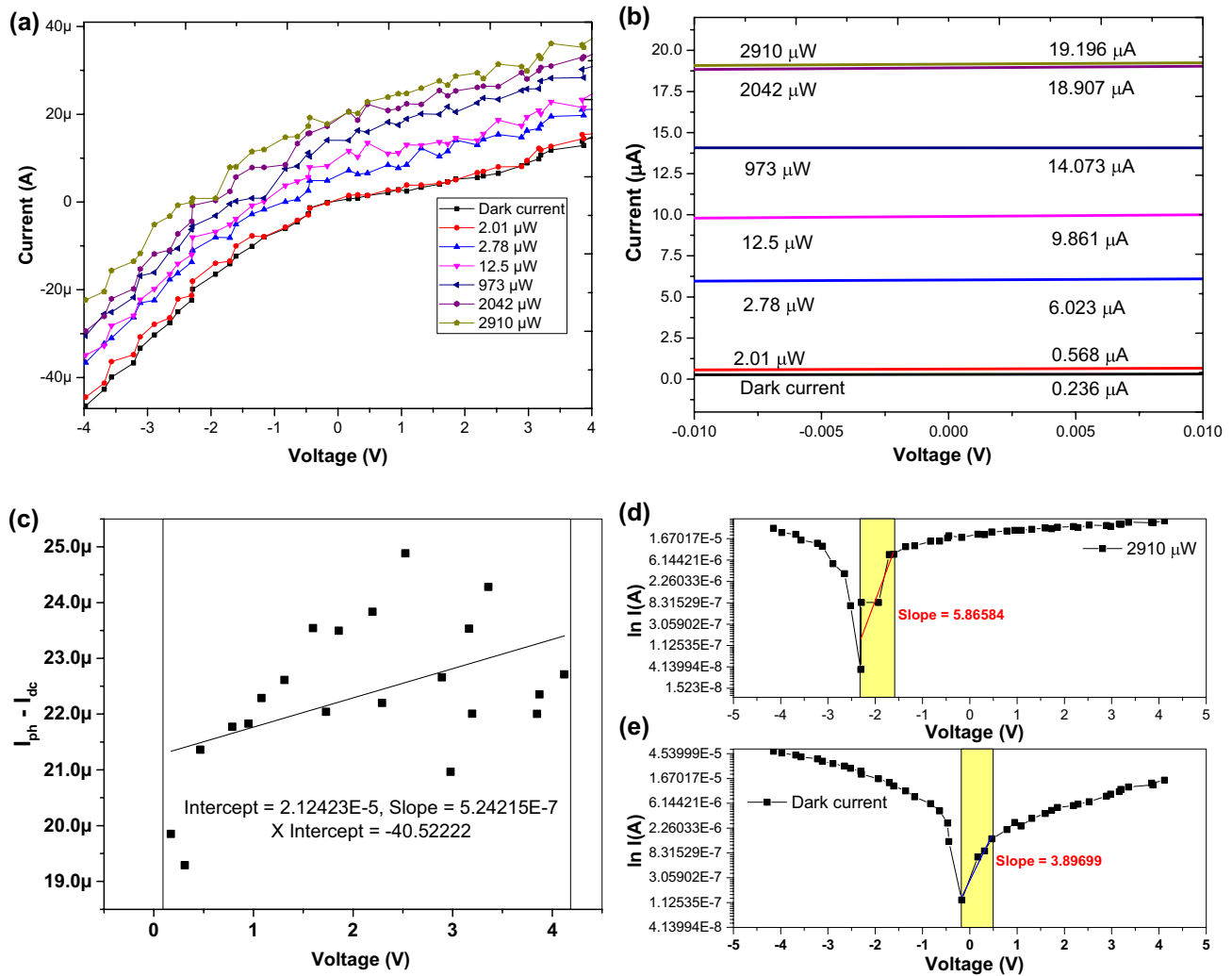


Fig. 4 I - V characteristics of C-ZnO hybrid thin film **a** DC bias voltage ranging from -4 to 4 V, **b** magnified version of I - V from -0.01 to 0.01 V, **c** distribution of photocurrent at $2910 \mu\text{W}$, **d** $\ln(I)$ of $2910 \mu\text{W}$ and **e** $\ln(I)$ of dark current

the p-Si region whereas the photogenerated holes moves and occupies the electropositive $\text{SiO}_2/\text{p-Si}$ region which is prone to capture the electrons. Thus, a good Schottky junction formed from the n-Si/C-ZnO hybrid thin film and $\text{SiO}_2/\text{p-Si}$ substrate of the heterojunction hybrid PD allows the separation of photogenerated e - h pairs which would in turn result in notable responsivity and response speed.

The PD would perform better with the introduction of an external electric field as it would provide additional drift on the photogenerated e - h pairs that favours the generation of a photocurrent. It can be seen from the I - V curve of Fig. 4a that a higher DC bias voltage results in a higher current. The differences between the generated photocurrent at $2910 \mu\text{W}$ and dark current is given in Fig. 4c. A possible linear fitting based on the distributed I - V points reveals a linear increase in photocurrent for DC biases ranging from zero to 4 V.

For a PD with Schottky behaviour, the presence of impurities and an interfacial layer effects the barrier height depending on the DC bias voltage. Based on the thermionic emission theory the ideality factor, η is best estimated from the equation $\eta = q/KT[(\partial V/\partial \ln(I))]$ using dark I - V characteristics at the intermediate current range where the shunt and series resistance are negligible (Sahatiya 2016; Sahatiya et al. 2018). The η value of the dark current is compared to that obtained under LED illumination at $2910 \mu\text{W}$, and measured from the linear slope of the forward bias region in Fig. 4d, e. The η value is determined to be 5.86 and 3.89 under $2910 \mu\text{W}$ illumination and dark current conditions, respectively. The increase in the η value indicates the high concentration of impurities and interface defects states in the C-ZnO structural matrix due to the incorporation of C NPs (Yakuphanoglu et al. 2010). The density of the surface states (D_s) is derived from the equation, $D_s = [\epsilon_i(\eta - 1)/t_i q^2]$

– (ϵ_{zn}/Wq^2) where ϵ_i and t_i are the dielectric constant and thickness of the interfacial layer respectively and have the values of 3.6 and 1.5 μm (Sahatiya et al. 2017). The dielectric constant of Zn is given by ϵ_{zn} with an assumed value of 10 (Jammula et al. 2015), while W is the depletion width of the depletion region and taken to be 160 nm (Saw et al. 2014). At η values of 5.86 and 3.89, the value of D_s is estimated to be 1.98×10^{44} and 1.05×10^{43} states/ m^2/eV under illumination at 2910 μW and dark current conditions, respectively. The barrier height, ϕ_B of the fabricated C–ZnO hybrid PD is calculated as $\phi_B = (kT/q)[\ln(AA^*T^2/I_0)]$ whereby kT/q is 0.02586 V and A^* is the effective Richardson constant of 0.0032 m^2/K^2 . The effective illumination area, A , is 2.5×10^{-5} m^2 while T is absolute room temperature and I_0 is reverse saturation current (Bedia et al. 2014). As the fabricated device is a bipolar due to the presence of both electron and holes, the I_0 is obtained from the forward bias region. Thus, the value of ϕ_B is computed to be 0.14 eV for the C–ZnO hybrid film PD. Two main parameters of the PD, the photoresponsivity $R_\lambda = (I_{pd} - I_{dk})/P$ and EQE = $hcR_\lambda/e\lambda$ are measured and calculated (Cheng et al. 2008; Zeng et al. 2010). I_{pd} and I_{dk} are the measured photocurrent and dark current, respectively, while P is the power of the beam onto the PD. The EQE is expressed as a percentage (Zhai et al. 2010a), with h being Planck’s constant, c the speed of light, e the electronic charge, λ the wavelength of illuminating beam and R_λ the measured photoresponsivity from the n-Si/C–ZnO hybrid thin film and SiO₂/p-Si heterojunction hybrid PD.

Figure 5a shows the photoresponsivity and photocurrent of the PD under 468 nm illumination. The highest photoresponsivity achieved is about 2.082/AW under 2.78 μW illumination, which is incomparable against available

commercial PDs. The fabricated C–ZnO hybrid PD exhibits selective characteristics towards light power 2.78 μW compared to lower power of 2.10 μW and high powers of 12.5, 973, 2042 and 2910 μW . The high photoresponsivity value represents a generation of larger photocurrent per unit incident power on the active area (Guo et al. 2017). The EQE is also found to be profound which yields a significant generation of electrons per unit incident photon, with all EQE values greater than 1% and significantly higher at 551 and 203% for light powers of 2.78 and 973 μW , respectively. This provides a source of electrons at per unit incident photon. Initially, the generation of $e-h$ pairs increases along with the light power, with saturation noted at about 18.671 and 18.960 μA for light powers of 2042 and 2910 μW , respectively. This shows that the device is able to operate at an optical light power range of 2000–3000 μW , due to saturation in carrier trapping and a reduction in the recombination barrier (Xie et al. 2012). Saturation of the photocurrent was observed to be at about 18.671 and 18.960 μA for light at powers of 2042 and 2910 μW , respectively. This shows that the device is able to operate optimally within a power range of 2000–3000 μW .

Furthermore, the temporal responses of the self-powered heterojunction hybrid PD are shown as in Fig. 6. The rise time is measured under both dark condition and also under illumination at 2910 μW . A non-saturated response can be seen as in Fig. 6 for high frequency modulations of 0.1, 1.0 and 10.0 kHz with spikes observed during the transition between the ON and OFF stages. Comparatively, low frequency modulations at 0.1, 1.0 and 10 Hz exhibit smoother transitions between the ON and OFF stages. These spikes could be due to the large surface area of the C–ZnO NWs with an average length to diameter ratio of 10

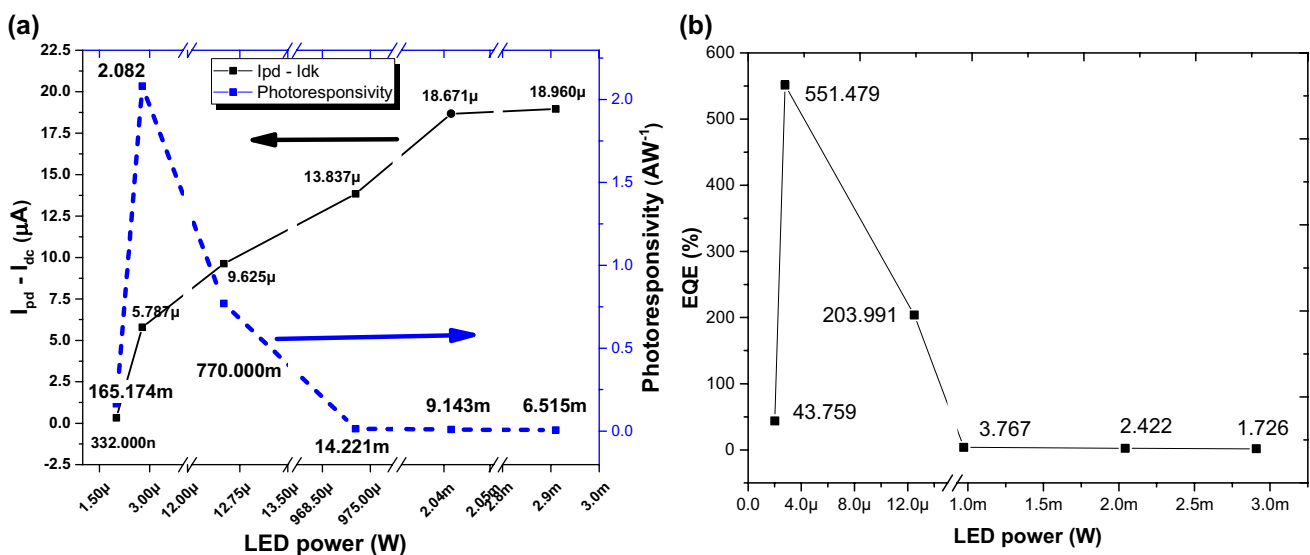


Fig. 5 a Photocurrent and photoresponsivity as a function of light power and b EQE of the self-powered PD at zero bias voltage

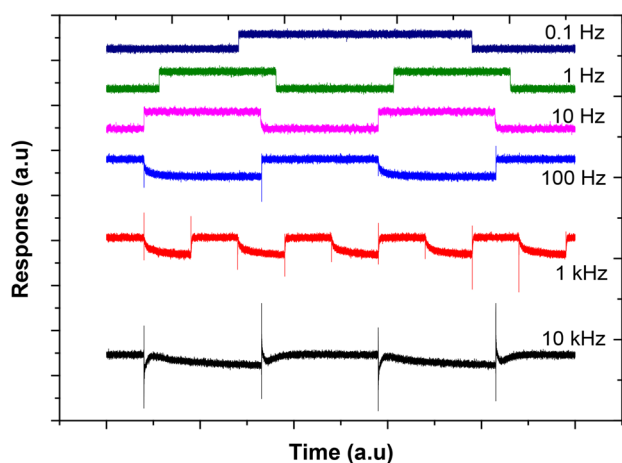


Fig. 6 Temporal response of self-powered n-Si/C-ZnO/SiO₂/p-Si heterojunction hybrid PD at zero bias voltage

as afore-mentioned. Moreover, some active surface defects would result in multilevel charge transitions which will slow down the recombination process of the electrons and holes (Tyagi et al. 2014; Yadav et al. 2007).

Due to the presence of spikes in Fig. 6, the Savitzky–Golay method is applied to eliminate the spikes and smoothen the temporal responses. This allows for a good estimation of the rise time, which is estimated to be within 9–12 μ s for frequency modulations of 0.01, 0.1, 1.0 and 10.0 kHz. This is shown in Fig. 7. This rise time is estimated to be lower than that obtained under slower modulation frequencies, such as 90 and 37 μ s at modulations to 0.1 and 1 Hz, respectively. Thus, the rise time shows an increasing trend as the frequency modulation increases, rising as the modulation frequency increases from 0.01 kHz \rightarrow 0.1 kHz \rightarrow 1 kHz. This fast transition response is agreeable with the carrier transport and energy band diagram of the n-Si/C-ZnO hybrid thin film and SiO₂/p-Si heterojunction hybrid PD as shown in Fig. 8. The ZnO NPs, which are in contact with the C NPs are energetically favourable for the transportation of photogenerated electrons from the conduction band to the valence band, which has an optical bandgap of \sim 3.28 eV as estimated in previous studies (Thandavan et al. 2014a). The reason for this is that the C NPs act as impurities in the ZnO NP structural matrix, creating point defects that alter the optical properties of ZnO (Tseng et al. 2014). The inclusion of the C NPs results in the bandgap becoming slightly decreased as compared to that of pristine ZnO (Morales-Torres et al. 2013), with the C NPs inducing sub energy levels in the bandgap of ZnO and allowing photogenerated holes already occupying this sub energy level to transit to the valence band. This leads to the expected reduced accumulation of electrons and further improves carrier transport efficiency to create the photocurrent. These

sub energy levels act as acceptors and indirectly favour the photoconduction mechanism in the C-ZnO hybrid thin film.

The n-Si and p-Si regions are connected to positive and negative terminal, respectively. As the PD is illuminated, the electrons drift through external circuit to the p-Si region. To accept those electrons, the sub-energy level acts as electron acceptors near the VBM. The electrons also trapped by the holes in the p-Si region and holes already formed in the ZnO energy band. It is worth mentioning that this device, the n-Si/C-ZnO/SiO₂/p-Si heterojunction self-powered PD is comparable in performance with other commercial PDs which typically have lower responsivity.

Commercial PDs such as gallium nitride (GaN), indium gallium nitride (InGaN) and AlGaN, silicon (Si) and silicon carbide (SiC) PDs work well in the ultraviolet (UV) region of 220–390 nm (Brown et al. 1993; Caria et al. 2001; Edmond et al. 1997; Osinsky et al. 1997). Similarly, indium gallium arsenide (InGaAs) PDs perform well in the wavelength region encompassing the UV to infrared (IR) sub-bands (Osinsky et al. 1998). The results obtained in this study showed that the proposed PD has a faster response time compared to titanium dioxide and MgZnO/PANI PDs which only exhibit rise times about 2 ms (Xu et al. 2018) and less than 3.0 s (Chen et al. 2016) for illumination at 250 nm, respectively. The slow O₂ adsorption/desorption processes on the ZnO film leads to long rise and fall times (Jin et al. 2016; Teng et al. 2016). Although, Yu et al. manage to get lower rise time of 4.50 μ s for Se/PANI PD using 610 nm light source, the fabricated Se/PPy and Se/PEDOT PDs results in relatively higher rise times of about 0.35 and 1.00 ms which are comparable to the 9.5 μ s of the proposed self-powered n-Si/C-ZnO/SiO₂/p-Si heterojunction hybrid PD of this work. A high photocurrent of around 19.19 μ A at zero bias voltage is also observed from the proposed PD of this work, which is substantially higher compared to other self-powered PDs that tend to show low photocurrents about 15.4 pA to 1.4 μ A (Wang et al. 2015; Yang et al. 2012; Yu et al. 2017). Thus, the same fabrication technique can be used to enhance the photoconduction properties of C-ZnO hybrid PD through the use of other materials such as Au and Ag NPs.

Conclusion

In this work, a novel self-powered C-ZnO hybrid PD based on an n-Si/C-ZnO hybrid thin film and SiO₂/p-Si heterojunction hybrid PD was successfully fabricated and demonstrated. This technique enabled C NPs to be scattered on the surface area of ZnO NWs to form tiny and long NWs approximately 10–100 nm in length. EDX analysis confirms the presence of C NPs within the ZnO NWs. The creation of point defects and sub-energy levels

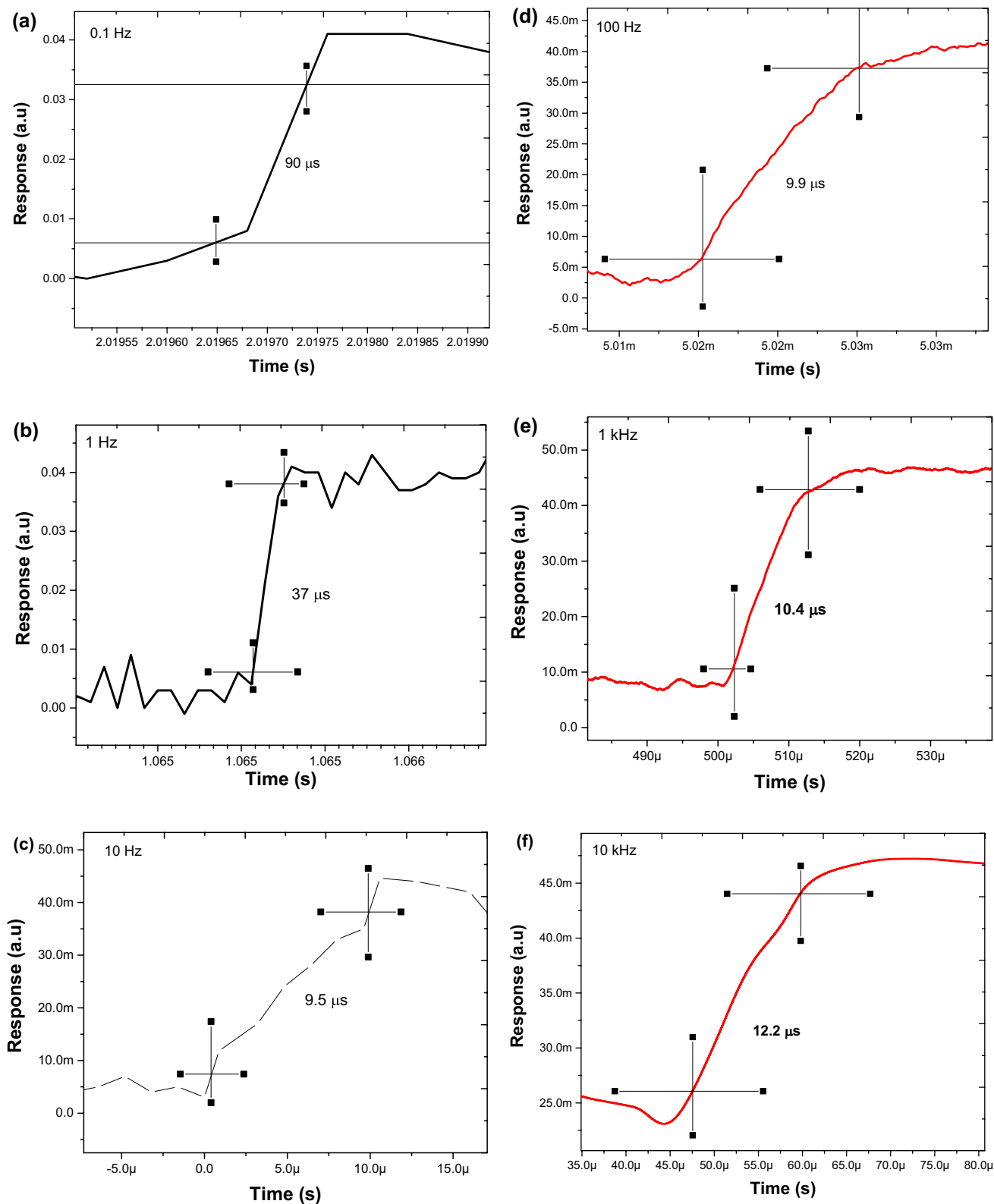


Fig. 7 Temporal response of rise time for frequency modulation of light at **a** 0.1 Hz, **b** 1.0 Hz, **c** 10.0 Hz, **d** 100.0 Hz, **e** 1.0 kHz and **f** 10.0 kHz

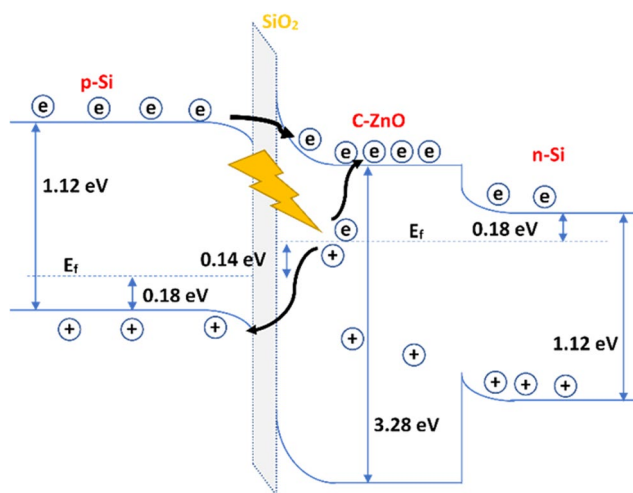


Fig. 8 Energy band diagram of n-Si/C-ZnO/SiO₂/p-Si heterojunction PD

by the C NPs in the lattices of ZnO has enhanced photodetection characteristics without any external power. The high rectifying ratio of 765 conditionally confirms a good Schottky junction between the Ag electrodes and the C-ZnO hybrid thin film. Moreover, illumination at 468 nm exhibits a fast response time around 9–12 μ s for frequency modulation ranged from 10 to 10,000 Hz. Photoresponsivity at 2.082/AW for light power of 2.78 μ W is among the highest values obtained for C-ZnO NW thin films while an EQE of 551% confirms that this self-powered heterojunction device would meet requirements for next generation energy efficient optoelectronic devices.

Acknowledgements Funding for this work was provided for by the Ministry of Higher Education, Malaysia under the Grants LRGS (2015) NGOD/UM/KPT and GA 010-2014 (ULUNG) as well as the University of Malaya under the Grants RU 001-2017.

References

- Ahmad H, Thandavan TMK, Ariannejad MM, Wu Yi C, Nor RM, Amiri IS (2017) Enhanced photoresponsivity from hybrid-ZnO nanowires with white LED 400–700-nm illumination. *IEEE J Quantum Electron* 53:1–6. <https://doi.org/10.1109/jqe.2017.2736253>
- Bedia A, Bedia F, Benyoucef B, Hamzaoui S (2014) Electrical characteristics of ultraviolet photodetector based on ZnO nanostructures. *Phys Procedia* 55:53–60
- Brown DM et al (1993) Silicon carbide UV photodiodes. *IEEE Trans Electron Devices* 40:325–333
- Brownson DA, Banks CE (2010) Graphene electrochemistry: an overview of potential applications. *Analyst* 135:2768–2778
- Caria M, Barberini L, Cadeddu S, Giannattasio A, Lai A, Rusani A, Sesselego A (2001) Far UV responsivity of commercial silicon photodetectors. *Nucl Instrum Methods Phys Res Sect A Accel Spectrom Detect Assoc Equip* 466:115–118
- Castiglioni C, Negri F, Rigolio M, Zerbi G (2001) Raman activation in disordered graphites of the A₁' symmetry forbidden $k \neq 0$ phonon: the origin of the D line. *J Chem Phys* 115:3769–3778
- Chen H-Y et al (2014) Realization of a self-powered ZnO MSM UV photodetector with high responsivity using an asymmetric pair of Au electrodes. *J Mater Chem C* 2:9689–9694
- Chen H, Yu P, Zhang Z, Teng F, Zheng L, Hu K, Fang X (2016) Ultrasensitive self-powered solar-blind deep-ultraviolet photodetector based on all-solid-state polyaniline/MgZnO bilayer. *Small* 12:5809–5816
- Chen D et al (2018) Ag₂S/ZnO core-shell nanoheterojunction for a self-powered solid-state photodetector with wide spectral response. *J Alloy Compd* 735:2491–2496
- Cheng J, Zhang Y, Guo R (2008) ZnO microtube ultraviolet detectors. *J Cryst Growth* 310:57–61
- Chrissanthopoulos A, Baskoutas S, Bouropoulos N, Dracopoulos V, Pouloupoulos P, Yannopoulos S (2011) Synthesis and characterization of ZnO/NiO p–n heterojunctions: ZnO nanorods grown on NiO thin film by thermal evaporation. *Photon Nanostruct Fundam Appl* 9:132–139
- Edmond J, Kong H, Suvorov A, Waltz D, Carter C Jr (1997) 6H-silicon carbide light emitting diodes and UV photodiodes. *Phys Stat Sol (A)* 162:481–491
- Ferrari AC (2007) Raman spectroscopy of graphene and graphite: disorder, electron–phonon coupling, doping and nonadiabatic effects. *Solid State Commun* 143:47–57
- Ferrari AC et al (2006) Raman spectrum of graphene and graphene layers. *Phys Rev Lett* 97:187401
- Garnier JRM, Parize R, Appert E, Chaix-Pluchery O, Kaminski-Cachopo A, Consonni V (2015) Physical properties of annealed ZnO nanowire/CuSCN heterojunctions for self-powered UV photodetectors. *ACS Appl Mater Interfaces* 7:5820–5829
- Guo Y, Li Y, Zhang Q, Wang H (2017) Self-powered multifunctional UV and IR photodetector as an artificial electronic eye. *J Mater Chem C* 5:1436–1442
- Huang D, Zhang M, Huang Q, Wang L, Tong K (2017) Mechanical property, oxidation and ablation resistance of C/C-ZrB₂-ZrC-SiC composite fabricated by polymer infiltration and pyrolysis with preform of Cf/ZrB₂. *J Mater Sci Technol* 33:481–486
- Jagadish C, Pearton SJ (2011) Zinc oxide bulk, thin films and nanostructures: processing, properties, and applications. Elsevier, Oxford
- Jammula RK, Pittala S, Srinath S, Srikanth VV (2015) Strong interfacial polarization in ZnO decorated reduced-graphene oxide synthesized by molecular level mixing. *Phys Chem Chem Phys* 17:17237–17245
- Jin Z et al (2016) Graphdiyne: ZnO nanocomposites for high-performance UV photodetectors. *Adv Mater* 28:3697–3702
- Khorasaninejad M, Walia J, Saini S (2012) Enhanced first-order Raman scattering from arrays of vertical silicon nanowires. *Nanotechnology* 23:275706
- Koppens F, Mueller T, Avouris P, Ferrari A, Vitiello M, Polini M (2014) Photodetectors based on graphene, other two-dimensional materials and hybrid systems. *Nat Nanotechnol* 9:780–793
- Kumar S, Sharma C (2017) Synthesis, characterization and catalytic performance of ZnO–CeO₂ nanoparticles in wet oxidation of wastewater containing chlorinated compounds. *Appl Nanosci* 7:567–575
- Kumar B, Gong H, Vicknesh S, Chua S, Tripathy S (2006) Luminescence properties of ZnO layers grown on Si-on-insulator substrates. *Appl Phys Lett* 89:141901
- Li G, Liu L, Wu G, Chen W, Qin S, Wang Y, Zhang T (2016) Self-powered UV–near infrared photodetector based on reduced graphene oxide/n-Si. *Vert Heterojunction Small* 12:5019–5026

- Liou Y-J, Huang W-J (2014) High temperature phase transitions of graphene oxide paper from graphite oxide solution. *J Mater Sci Technol* 30:1088–1091
- Liu F et al (2014) High-sensitivity photodetectors based on multilayer GaTe flakes. *ACS Nano* 8:752–760
- Lopez-Sanchez O, Lembke D, Kayci M, Radenovic A, Kis A (2013) Ultrasensitive photodetectors based on monolayer MoS₂. *Nat Nanotechnol* 8:497–501
- Low T, Rodin A, Carvalho A, Jiang Y, Wang H, Xia F, Neto AC (2014) Tunable optical properties of multilayer black phosphorus thin films. *Phys Rev B* 90:075434
- Morales-Torres S, Pastrana-Martínez LM, Figueiredo JL, Faria JL, Silva AM (2013) Graphene oxide-P25 photocatalysts for degradation of diphenhydramine pharmaceutical and methyl orange dye. *Appl Surf Sci* 275:361–368
- Mridha S, Basak D (2007) Ultraviolet and visible photoresponse properties of n-Zn O/p-Si heterojunction. *J Appl Phys* 101:083102
- Ning Y, Zhang Z, Teng F, Fang X (2018) Novel transparent and self-powered UV photodetector based on crossed ZnO nanofiber array homojunction. *Small* 14:1703754
- Niu G et al (2016) Photodetection in hybrid single-layer graphene/fully coherent germanium island nanostructures selectively grown on silicon nanotip patterns. *ACS Appl Mater Interfaces* 8:2017–2026
- Nusir AI, Manasreh M (2015) Self-powered near-infrared photodetector based on asymmetrical Schottky interdigital contacts. *IEEE Electron Device Lett* 36:1172–1175
- Osinsky A, Gangopadhyay S, Gaska R, Williams B, Khan MA, Kuksenkov D, Temkin H (1997) Low noise p- π -n GaN ultraviolet photodetectors. *Appl Phys Lett* 71:2334–2336
- Osinsky A, Gangopadhyay S, Lim B, Anwar M, Khan MA, Kuksenkov D, Temkin H (1998) Schottky barrier photodetectors based on AlGaIn. *Appl Phys Lett* 72:742–744
- Ouyang B, Zhang K, Yang Y (2018) Photocurrent polarity controlled by light wavelength in self-powered ZnO nanowires/SnS. *Photodetect Syst Sci* 1:16–23
- Radisavljevic B, Radenovic A, Brivio J, Giacometti iV, Kis A (2011) Single-layer MoS₂ transistors. *Nat Nanotechnol* 6:147–150
- Rajalakshmi M, Arora AK, Bendre B, Mahamuni S (2000) Optical phonon confinement in zinc oxide nanoparticles. *J Appl Phys* 87:2445–2448
- Sahatiya P, Badhulika S (2015) One-step in situ synthesis of single aligned graphene–ZnO nanofiber for UV sensing. *RSC Adv* 5:82481–82487
- Sahatiya P, Badhulika S (2016) UV/ozone assisted local graphene (p)/ZnO (n) heterojunctions as a nanodiode rectifier. *J Phys D Appl Phys* 49:265101
- Sahatiya P, Jones SS, Gomathi PT, Badhulika S (2017) Flexible substrate based 2D ZnO (n)/graphene (p) rectifying junction as enhanced broadband photodetector using strain modulation 2D. *Materials* 4:025053
- Sahatiya P, Shinde A, Badhulika S (2018) Pyro-phototronic nanogenerator based on flexible 2D ZnO/graphene heterojunction and its application in self-powered near infrared photodetector and active analog frequency modulation. *Nanotechnology* 29:325205
- Saw KG, Tneh SS, Yam FK, Ng SS, Hassan Z (2014) Determination of acceptor concentration, depletion width, donor level movement and sensitivity factor of ZnO on diamond heterojunction under UV illumination. *PLoS One* 9:e89348
- Scott J (1970) UV resonant Raman scattering in ZnO. *Phys Rev B* 2:1209
- Teng FB, Zheng L, Hu K, Chen H, Li Y, Zhang Z, Fang X (2016) A surface oxide thin layer of copper nanowires enhanced the UV selective response of a ZnO film photodetector. *J Mater Chem C* 4:8416–8421
- Teng FA, Ouyang W, Li Y, Zheng L, Fang X (2017) Novel structure for high performance UV photodetector based on BiOCl/ZnO. *Hybrid Film small* 13:1700156
- Thandavan TMK, Gani SMA, Wong CS, Nor RM (2014a) Synthesis of ZnO nanowires via hotwire thermal evaporation of brass (CuZn) assisted by vapor phase transport of methanol. *J Nanomater* 2014:1–10. <https://doi.org/10.1155/2014/105875>
- Thandavan TMK, Wong CS, Gani SMA, Nor RM (2014b) Photoluminescence properties of un-doped and Mn-doped ZnO nanostructures. *Mater Express* 4:475–482
- Tseng L et al (2014) Green emission in carbon doped ZnO films. *AIP Adv* 4:067117
- Tyagi M, Tomar M, Gupta V (2014) Fabrication of an efficient GLAD-assisted p-NiO nanorod/n-ZnO thin film heterojunction UV photodiode. *J Mater Chem C* 2:2387–2393
- Van Schalkwyk L, Meyer W, Auret FD, Nel JM, Ngoepe PNM, Diale M (2012) Characterization of AlGaIn-based metal–semiconductor solar-blind UV photodiodes with IrO₂ Schottky contacts. *Phys B Condens Matter* 407:1529–1532
- Wagner P, Helbig R (1974) Halleffekt und anisotropie der beweglichkeit der elektronen in ZnO. *J Phys Chem Solids* 35:327–335
- Wang ZL (2004) Nanostructures of zinc oxide. *Mater Today* 7:26–33
- Wang H, Yi G, Zu X, Jiang X, Zhang Z, Luo H (2015) A highly sensitive and self-powered ultraviolet photodetector composed of titanium dioxide nanorods and polyaniline nanowires. *Mater Lett* 138:204–207
- Xie X et al (2012) Visible–NIR photodetectors based on CdTe nanoribbons. *Nanoscale* 4:2914–2919
- Xu J, Yang W, Chen H, Zheng L, Hu M, Li Y, Fang X (2018) Efficiency enhancement of TiO₂ self-powered UV photodetectors using a transparent Ag nanowire electrode. *J Mater Chem C* 6:3334–3340
- Yadav HK, Sreenivas K, Gupta V (2007) Enhanced response from metal/ZnO bilayer ultraviolet photodetector. *Appl Phys Lett* 90:172113
- Yakuphanoglu F, Caglar Y, Caglar M, Ilcan S (2010) ZnO/p-Si heterojunction photodiode by sol–gel deposition of nanostructure n-ZnO film on p-Si substrate. *Mater Sci Semicond Process* 13:137–140
- Yang S, Gong J, Deng Y (2012) A sandwich-structured ultraviolet photodetector driven only by opposite heterojunctions. *J Mater Chem* 22:13899–13902
- Ye J, Tripathy S, Ren F-F, Sun X, Lo G, Teo K (2009) Raman-active Fröhlich optical phonon mode in arsenic implanted ZnO. *Appl Phys Lett* 94:011913
- Yu P, Hu K, Chen H, Zheng L, Fang X (2017) Novel p–p heterojunctions self-powered broadband photodetectors with ultrafast speed and high responsivity. *Adv Func Mater* 27:1703166
- Zeng H, Duan G, Li Y, Yang S, Xu X, Cai W (2010) Blue luminescence of ZnO nanoparticles based on non-equilibrium processes: defect origins and emission controls. *Adv Func Mater* 20:561–572
- Zhai T et al (2010a) Fabrication of high-quality In₂Se₃ nanowire arrays toward high-performance visible-light photodetectors. *ACS Nano* 4:1596–1602
- Zhai T, Li L, Wang X, Fang X, Bando Y, Golberg D (2010b) Recent developments in one-dimensional inorganic nanostructures for photodetectors. *Adv Func Mater* 20:4233–4248
- Zhang D, Liu C, Li K, Chen Y, Ruan S, Zhang X, Li C (2018) Facilitated extrinsic majority carrier depletion and photogenerated exciton dissociation in an annealing-free ZnO: C photodetector. *Nanoscale* 10:6459–6466
- Zhao B, Wang F, Chen H, Zheng L, Su L, Zhao D, Fang X (2017) An ultrahigh responsivity (9.7 mA W⁻¹) self-powered solar-blind photodetector based on individual ZnO–Ga₂O₃. *Heterostruct Adv Funct Mater* 27:1700264